JOURNAL OF QUATERNARY SCIENCE (2026) **41**(2) 316–332 ISSN 0267-8179. DOI: 10.1002/jqs.70043

JQS Journal of Quaternary Science QRA Quaternary Research Association

Holocene climate oscillations, seismotectonic events and human–environmental interactions reconstructed from the Giannades palaeolake on Corfu (Eastern Mediterranean, Greece)

ESRA REICHERT,[1] PETER FISCHER,[1]* BERND ZOLITSCHKA,[2] TINA GEORG,[1] LEA OBROCKI,[1] DENIS SCHOLZ,[3] KATJA SPORN[4] and ANDREAS VÖTT[1]
[1]Institute of Geography, Johannes Gutenberg-Universität, Mainz, Germany
[2]Institute of Geography, GEOPOLAR, University of Bremen, Bremen, Germany
[3]Institute for Geosciences, Johannes Gutenberg-Universität, Mainz, Germany
[4]Deutsches Archäologisches Institut, Athens, Greece

Received 27 January 2025; Revised 24 November 2025; Accepted 4 December 2025

ABSTRACT: The Mediterranean is particularly sensitive to rapid climate changes (RCCs) during the Holocene. An increasing number of natural climate archives revealed that socio-economic developments were influenced by such RCCs since the Palaeolithic. However, multi-millennial and high-resolution archives are still rare and often located in mountainous regions, where they do not represent environmental conditions close to human settlements. Here, we present a 16 m-long Holocene sediment record from the Giannades coastal palaeolake on Corfu, western Greece, which combines multiproxy analyses including high-resolution X-ray fluorescence core scanning with a robust radiocarbon-based age–depth model. A mean sedimentation rate of 1.6 mm/a characterises this lake record from 10.59 cal ka BP (basal age) until it started to desiccate around 1.8 cal ka BP. The environmental conditions of the Giannades palaeolake document a sensitivity to RCCs during the Early and Mid-Holocene correlating with sapropel S1 of the Mediterranean Sea and with the 8.2 ka event of the North Atlantic. Furthermore, signals of local to regional seismotectonic events were recorded, as evidenced by comparison with data from geomorphological and geoarchaeological studies of other coastal sites on Corfu. After a period of stability during the early Late Holocene, a two-phased desiccation started at 2.3 cal ka BP. This is coincident with a prominent seismotectonic event of the fourth/third century BCE, but also with the Roman Warm Period and related human landscape modifications.

KEYWORDS: Corfu Island; co-seismic events; Giannades palaeolake; Holocene rapid climate changes; palaeoclimate

Introduction

The Mediterranean region is sensitive to rapid climate changes (RCCs) due to its position at the boundary between two major climate regimes: the North Atlantic-dominated temperate regime over Central Europe and the descending branch of the Hadley cell over northern Africa (Lolis et al., 2002; Rohling et al., 2019). RCCs occurred six times globally in the Holocene, roughly during the periods 9.0–8.0 cal ka BP, 6.0–5.0 cal ka BP, 4.2–3.8 cal ka BP, 3.5–2.5 cal ka BP, 1.2–1.0 cal ka BP and 0.6–0.15 cal ka BP, and were typically associated with polar cooling, tropical aridity and global circulation pattern changes (Mayewski et al., 2004). However, regional expressions of Holocene RCCs vary. In the Mediterranean, they are characterised by an increased wintertime influx of cold and dry northerly polar/continental air masses, which reach the Mediterranean through gaps in the mountain ranges of the Alps, likely caused by an intensification of the Siberian High. Despite the high thermal capacity of water, sea surface temperatures (SSTs) in the Aegean and Adriatic Seas dropped by over 2°C during RCC events (Rohling et al., 2019), implying even more pronounced conditions over land. Rohling et al. (2009) hypothesise that these polar air outbreaks manifested as extremely cold and dry conditions upwind of evaporative water bodies, whereas downwind, they would bring less pronounced cold conditions and increased precipitation.

In addition to RCCs, multi-millennial-scale trends have been identified in numerous regional archives. Finné et al. (2019) compiled 47 Holocene climate records from the Mediterranean and found a generally wetter Early to Mid-Holocene and a drier Mid- to Late Holocene in five out of six statistically determined regions.

Precise knowledge of Mediterranean climate patterns during the Holocene is important because of the rich history of human occupation in a region where climatic conditions are considered important drivers for socio-economic developments in ancient societies (Berger and Guilaine, 2009). Prominent examples from lacustrine environments that span most or all of the Holocene and are sensitive to climate variability include Lake Ohrid and Lake Prespa on the border between Macedonia and Albania (Lacey et al., 2015), Vouliagmeni Lake at the Gulf of Corinth (Emmanouilidis et al., 2022) and Lake Ioannina in northwestern Greece (Frogley et al., 2001; Fig. 1). Data from such records are compared with high-resolution marine sediment cores that allow, for example, the reconstruction of SSTs and palaeoenvironmental events that impacted the Mediterranean Sea (e.g., Geraga et al., 2008; Siani et al., 2013; Rohling et al., 2019).

*Correspondence: Peter Fischer, as above.
Email: fischep@uni-mainz.de

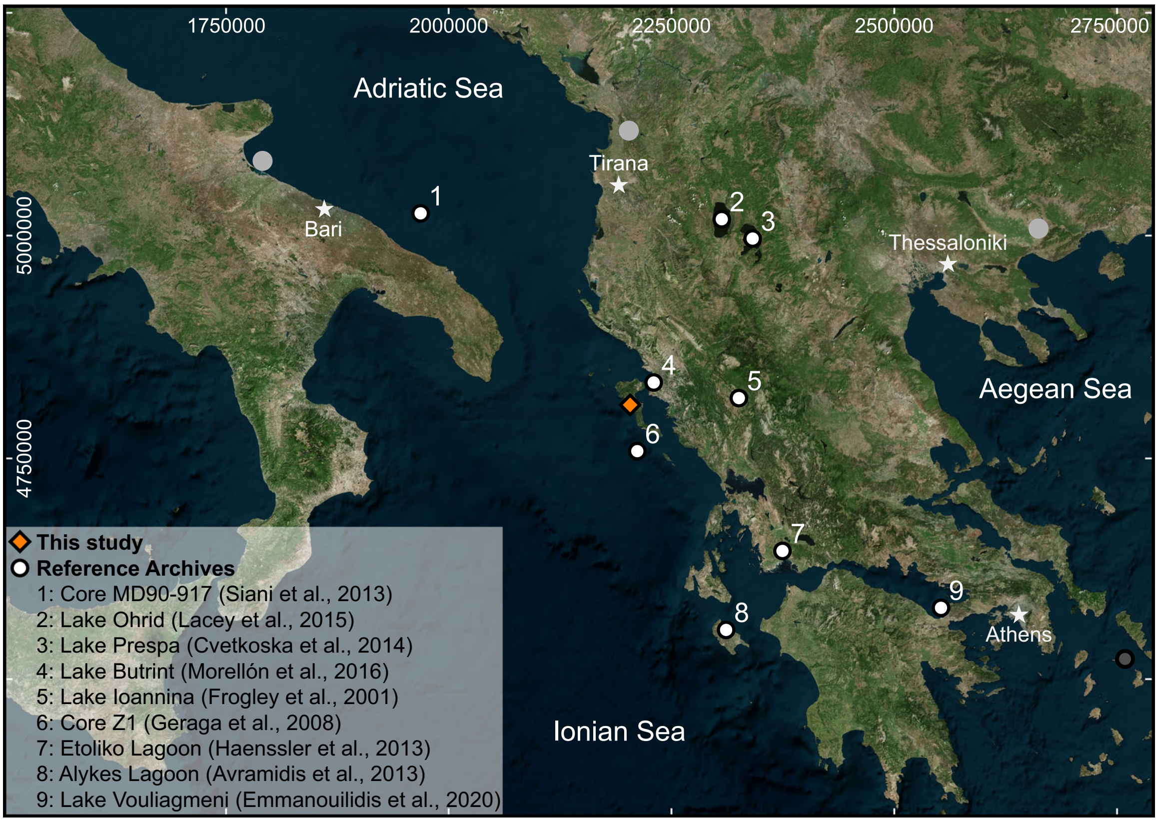

Figure 1. Overview of regional archives of Holocene palaeoenvironmental and palaeoclimatic change. The orange diamond shows the study site of the Giannades Polje on Corfu Island (cp. Fig. 2). [Color figure can be viewed at wileyonlinelibrary.com]

In addition, near-coast terrestrial and lacustrine archives are abundant (Fig. 1), for example, Lake Butrint (Morellón et al., 2016), Alykes Lagoon (Avramidis et al., 2013) and Etoliko Lagoon (Vött et al., 2007; Haenssler et al., 2013). However, these archives are often sensitive to seismic, anthropogenic and local geomorphological effects and thus more difficult to interpret in terms of climate.

Numerous coastal studies focus on effects such as tsunami inundation of lagoonal sites (Finkler et al., 2018a, 2019; Obrocki et al., 2020), relative sea-level changes (Vött, 2007; Finkler et al., 2018b) or anthropogenic impacts (Jahns, 2005; Vött et al., 2009; Finkler et al., 2018a, 2019), but few near-coastal sites that cover the majority of the Holocene are investigated in terms of climate. One example of such records is the Lake Vouliagmeni record in the Gulf of Corinth (Fig. 1; Emmanouilidis et al., 2022). Here, we present a new palaeolake archive from the Giannades polje on Corfu Island, Greece. This high-resolution record provides detailed insights into environmental conditions close to the coast of the Ionian Sea. Based on a multiproxy approach, we aim to detect variations in sediment sources, biological activity, oxic and anoxic bottom water conditions and carbonate precipitation to identify changes in environmental conditions for a better understanding of regional climatic and seismotectonic events.

Regional setting of Corfu

Natural conditions and climate

Corfu is the northernmost island of the Ionian archipelago and the closest to the Strait of Otranto, where the Ionian Sea meets the Adriatic Sea. The study site is part of a polje, a typical flat-bottomed basin in a karstic landscape with limited surface drainage. We will hereafter refer to the site as Giannades Polje (also called Ropa Valley). The polje (Fig. 2(A)) occupies a NNW–SSE-extending half-graben structure (9 km long, up to 2.5 km wide), delimited to the east by the Ionian Thrust, where Triassic gypsum breccias overlie Pliocene marls that make up most of the polje's base. To the west, bedrock is composed of Pliocene conglomerates and flysch, the latter representing a sedimentary sequence of sandstones and mudstones associated with orogenetic processes, both forming an approximately 300-m-high ridge separating the polje from the Ionian Sea (IGME, 1970). A narrow gap near the village of Ermones drains the polje into the sea at 33 m a.s.l. and presumably limited the maximum lake level during the Holocene, before the basin was silted up and the lake desiccated. Our study area is located ca. 1 km east of the outlet (Fig. 2(B),(C)).

The entire region is characterised by seismotectonic activity. Evelpidou and Pirazzoli (2014) and Mastronuzzi et al. (2014) investigated the complex history of seismic uplift and submergence based on palaeo-shorelines and found frequent Late Holocene events. Finkler et al. (2018b, 2019) describe sedimentary evidence of co-seismic uplift, tsunami landfall and related harbour destruction associated with a seismic event in the fourth/third century BCE that also destroyed the famous Temple of Hera in ancient Corfu City (Sapirstein, 2012).

Corfu is located close to the continent–continent collision zone between the Adriatic Microplate and the Eurasian plate to the north, to the two subduction zones of the Calabrian Arc to the southwest and the Hellenic Arc to the southeast (van Hinsbergen et al., 2006). These tectonic systems are separated by the Cefalonia Transform Fault to the south of the island (Kokkalas et al., 2006). Corfu experiences frequent earthquakes and uplift/subsidence events due to its position in this stress field (van Hinsbergen et al., 2006; Kokkalas et al., 2006). Such a setting presents serious challenges for the study of climate archives due to potential seismic disturbances of sedimentary

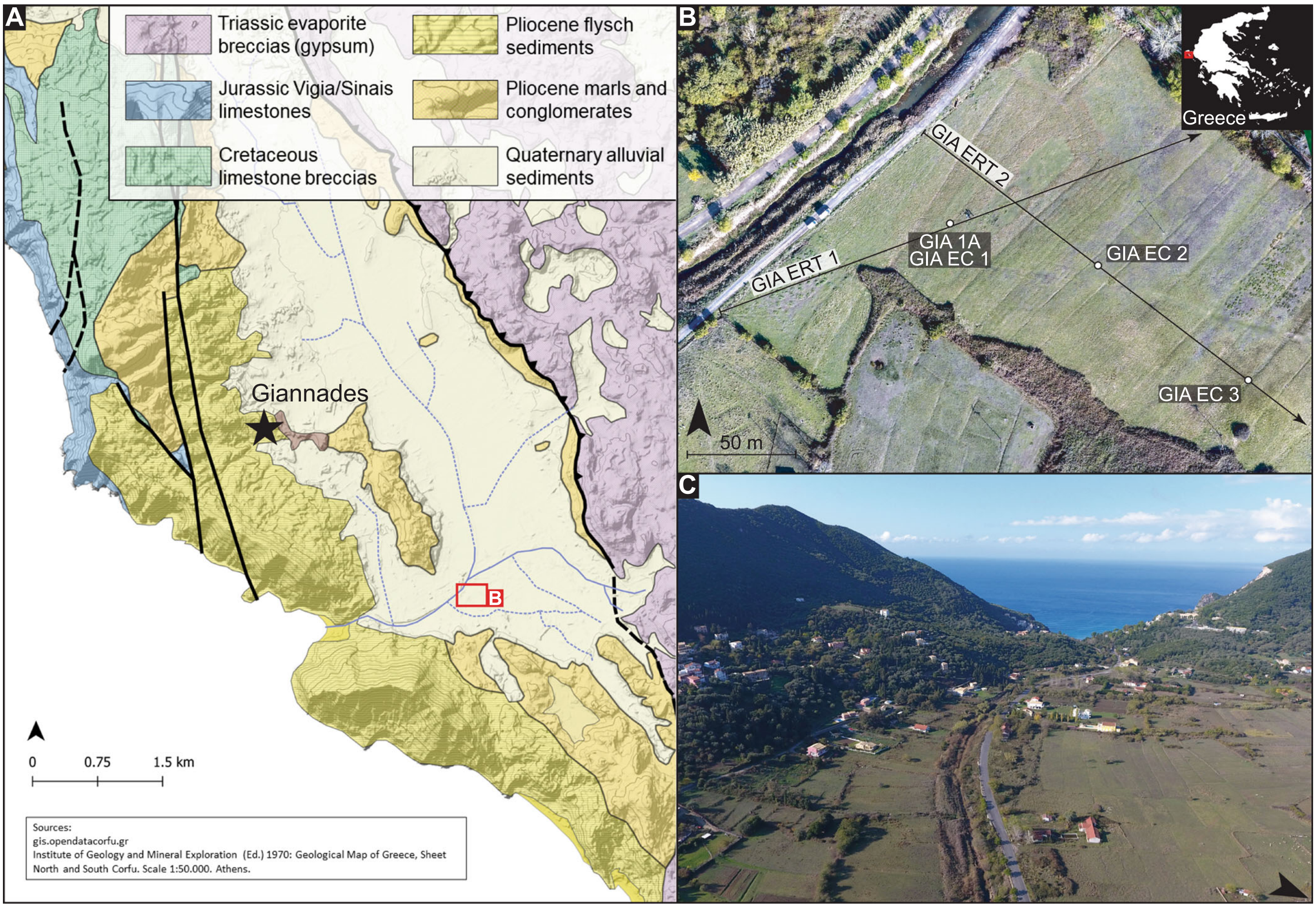

Figure 2. (A) Geological map of the Giannades Polje on Corfu, modified after IGME (1970), overlain by a shaded relief map (gis.opendatacorfu.gr). (B) Drone image of the study site showing the location of transects GIA ERT 1 and GIA ERT 2, locations of direct-push electrical conductivity (EC) measurements and coring site GIA 1A. The inset map shows the location of Corfu as northernmost Ionian Island in Greece. (C) Drone image with view towards the gap in the Pliocene bedrock ridge to the west of the coring site. [Color figure can be viewed at wileyonlinelibrary.com]

records (Morellón et al., 2016), while considerable research into natural hazards is focussed on the Greek coastal regions because of the seismicity (Vött, 2007; Fischer et al., 2016a; Finkler et al., 2018a, 2018b, 2019; Obrocki et al., 2020).

The climate of Corfu is characterised by hot, arid summers and mild, rainy winters, with most of the annual rainfall occurring between November and March. The average annual precipitation and the average annual temperature were 1027 mm and 16.53°C for the period 1990–2020, respectively (www.climateknowledgeportal.worldbank.org, 2025). The alteration between arid summers and rainy winters results from planetary and solar parameters causing a seasonal shift of the boundary between the wet-temperate climate regime over Central Europe and the sub-tropical climate over northern Africa caused by the descending branch of the Hadley cell. The boundary moves north in summer, bringing stable high-pressure conditions, and is pushed south in winter, allowing cyclogenesis and heavy rains (Lolis et al., 2002).

History of human occupation

Corfu has been inhabited by humans since the Middle Palaeolithic (Sordinas, 1969; Ferentinos et al., 2012). Following Weninger et al. (2009), one must assume that RCC-related climatic deterioration plays a crucial role for social change, although the interplay between Early to Mid-Holocene climate and prehistoric societies in the Eastern Mediterranean remains poorly understood.

Regarding potential impacts of RCCs on the cultural evolution, Berger et al. (2016) suggest that the RCC related to the 8.2 ka event strongly influenced the Mesolithic–Neolithic transition on Corfu. Based on the investigation of sedimentary sequences at the Sidari coastal plain in northern Corfu Island, these authors assume that the 8.2 ka event caused increased erosion due to severe or extreme rainfall events, forcing Neolithic populations to relocate.

In classical times, Corfu's position south of the Strait of Otranto made it highly valuable to seafaring societies, both commercially and strategically (Kiechle, 1979). Corinthian colonists founded the city of Corcyra in 730 BCE and displaced the Eretrians. They became a dominant seafaring power and undertook the first recorded naval battle in Greek history against their metropolis in 664 BC (Thucydides 1.13.4, after Dent, 1910). Its strategic position made Corfu a key naval base throughout classical antiquity and caused it to be frequently attacked by other powers.

Materials and methods

Field work

Geophysical measurements and sediment coring were accomplished in October 2017 near the village of Giannades (Fig. 2). Geophysical site prospection was carried out to determine the stratigraphy of the shallow subsurface. Electrical resistivity tomography (ERT) transects were measured using a multi-electrode device (type Syscal R1 Plus Switch 48, Iris Instruments) and a Wenner–Schlumberger electrode array with 5 m electrode spacing. To calibrate ERT measurements and gain high-resolution subsurface data, three Direct Push Electrical Conductivity (EC) measurements were performed using a Geoprobe SC520 soil conductivity probe adapted to a Nordmeyer drill rig RS 0/2.3 using a Wenner electrode array (Fischer et al., 2016b). EC data were then linearly detrended based on visual matching with the closely related Ti/Ca ratio. The resulting unitless values were normalised to zero mean and unit standard deviation.

A relatively homogeneous subsurface structure was identified and ensured the retrieval of sediments without channel deposits or other disturbances. The 16-m-long sediment core, GIA 1 A, was retrieved with the Nordmeyer drill rig in segments of 1 m using a closed steel auger system (diameter: 63 mm) and plastic liners (diameter: 50 mm). Due to sediment loss and compression, the core has small gaps, especially in its upper part. Core recovery rates for each coring metre are shown in Table A1 in the appendix.

Positions and elevations were measured using a Topcon differential GPS HiPerPRO FC-250 with a precision better than 2 cm.

Laboratory work

Sediment-filled liners were cut into halves, photographed and described in terms of sedimentological characteristics (Jahn et al., 2006). Smear slides were created throughout the core after Rothwell (1989) to qualitatively determine the sediment composition. Magnetic susceptibility (MS) was measured with a Bartington MS2K surface sensor at intervals of 1 cm to detect changes in Fe-bearing minerals. Seventy-six samples were analysed for grain size using the Köhn method (Köhn, 1929) following the procedures of Obrocki et al. (2020).

Total carbon (TC) and total nitrogen (TN) concentrations were measured for 31 samples using an Elementar Vario EL Cube. Samples were dried at 40°C for at least 24 h and ground with a ball mill before weighing out 10 mg for TC and TN measurements and 13 mg for measurements of total inorganic carbon (TIC) after burning at 550°C for 4 h. Total organic carbon (TOC) was determined by subtracting TIC from TC. TOC is an important indicator of lake trophic state, as it represents the amount of organic carbon that was not decomposed, and TOC/TN ratios indicate organic matter origins, with high TOC/TN ratios found in terrestrial plants and low values in non-emergent macrophytes and algae (Meyers and Ishiwatari, 1993).

High-resolution X-ray fluorescence (XRF) scanning took place at the GEOPOLAR lab (University of Bremen) with a Cox Analytics ITRAX XRF core-scanner using a chromium tube set at 30 kV and 50 mA with an exposure time of 5 s and a step size of 1 mm. For every 1-m section, at least three 25-mm subsections were measured in triplicate to allow for repeatability assessments. Thirty-six elements were determined in counts (cts). Additionally, variations of coherent (coh) and incoherent (inc) radiation scattering were given as unitless values.

The XRF data set was cleaned for gaps resulting from dehydration cracks. Using the triplicate measurements and Pearson correlation coefficients (PCC) for evaluation, nine elements (Sr, Ca, S, Ti, Fe, Rb, Mn, K and Si) were selected for interpretation based on high repeatability and low signal to noise ratios. These elements were used as proxies for lake environmental conditions, as they indicate both sediment composition and chemical processes that took place during sediment deposition or diagenesis. For comparability and noise removal, elemental ratios and elemental curves were smoothened with a 51-point running average.

The selected elements were normalised as centred log ratios (clr) (Fig. S7) to eliminate the effects of dilution and changes in physical properties throughout the core (e.g., Bertrand et al., 2024):

$$\text{clr of } I_{ij} = \ln(I_{ij}/gm_j),$$

where I_{ij} is intensity I of element i at point j and gm_j is the geometric mean of all values selected at point j (Weltje et al., 2015).

A series of Pearson correlation matrices were computed for the XRF data set with the addition of the inc/coh ratio to detect relationships between elements in different sections of the core. PCCs were calculated between every pair of components for 311 sections of 50 mm. Sections containing less than 10 data points were excluded. The PCCs allow interpretation of changes in biogeochemical processes as elemental pairs co-vary or become independent from one another throughout the core.

Chronology

Eleven radiocarbon dating samples of terrestrial plant remains were dated at the Curt-Engelhorn-Zentrum für Archäometrie gGmbH in Mannheim, Germany. An acid–base–acid pretreatment using HCl, NaOH and again HCl was performed before samples were measured using a MICADAS accelerator mass spectrometer. Ages were calibrated using Calib 8.2 software based on the IntCal20 calibration curve (Reimer et al., 2020), and the chronology was created with the R-package 'rbacon' (Blaauw et al., 2011). Due to the complex lithology of the core, a unit-related stratigraphy was not constructed. The uppermost 1.6 m of the core was interpreted as strongly reworked and is regarded as an event deposit for the purpose of computing the age–depth model.

Results

Stratigraphy

Electrical resistivity tomography transects (Figs. 2(B) and 3) were measured prior to coring to identify the thickest sedimentary sequence. GIA ERT 1 (Fig. 3) shows a subdivision into an upper low-resistivity unit (Unit A < 13 Ωm) and a lower unit with significantly higher values (Unit B > 13 Ωm). Direct Push measurement GIA EC 1 shows consistently high values from 2 m b.s. (below surface) downwards (mean 129 mS/m), with a distinct minimum between 13.5 and 14.0 m decreasing to a mean of 68 mS/m. In transect GIA ERT 2, unit A is limited to the NW part, while towards the SE, unit B increasingly reaches the surface. This is also reflected by GIA EC 2 and GIA EC 3, which show consistently lower conductivity values (both with a mean of 51 mS/M).

Sediment core GIA 1 A (35.90 m a.s.l., Figs. 2(B) and 4) shows a near-continuous depositional environment interrupted by an erosional unconformity at 13.78 m b.s. Bedrock was not reached during coring. The core is dominated by silt and clay, is sometimes finely laminated and does not show signs of high-energy disturbances. Towards the surface, a transition to anthropogenically altered sediments terminates the record. The main sources of sediment are precipitation of dissolved Ca from the water column, organic matter and slope run-off eroding local Pliocene marls that form the ridge delimiting the polje to the west. The Giannades Polje record is divided into six reoccurring lithological units (I–VI). Each unit is characterised by similar geochemical features, elemental relationships, organic content and visual characteristics (Figs. 4–6; Table 1). Subunits are indicated by lower case letters.

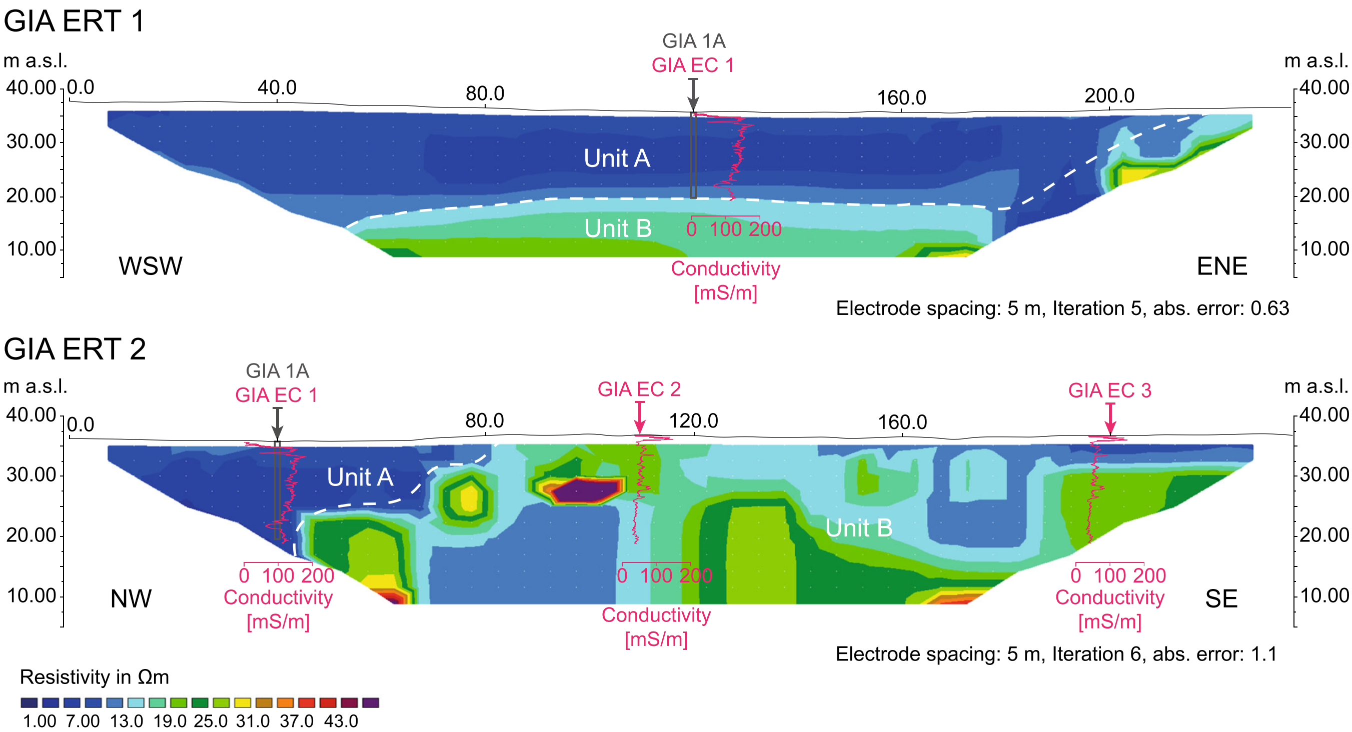

Figure 3. Depth section of transects GIA ERT 1 (top) and GIA ERT 2 (bottom) differentiating the shallow subsurface in two units. Unit A is characterised by low resistivities, while unit B shows significantly higher values. Direct-Push (DP) measurement GIA EC 1 indicates a 16 m thick sequence of low resistivity throughout the entire sequence below 1 m, while GIA EC 2 and GIA EC 3 show significantly lower EC values in line with ERT results. [Color figure can be viewed at wileyonlinelibrary.com]

Unit I

This unit is the most common lithological unit of GIA 1A and is dominated by greyish to light greyish silty clay loam. Subunits Ia–Ic are classified according to sedimentary features (Table 1). Overall, it is characterised by precipitated carbonates, slope-borne clastics and organic matter. Ca and Ti are negatively correlated, and Fe and Ti are positively correlated (Fig. 5). S tends to correlate negatively with Fe and shows a weak to absent correlation with Ca (Fig. 5). MS is low and organic matter content ranges from 2% to 8% (Fig. 5). Pyrite is abundant, and gastropods, ostracods and diatoms are present in variable abundance (Fig. S1). Subunits Ib and Ic are laminated, showing a distinct dichotomy between light calcite layers and dark grey to brown, clay-rich clastic layers, while subunit Ia is more homogeneous. EC shows minor fluctuations apart from Ib between 13.78 and 13.16 m, where it distinctly increases towards the top.

Unit II

The subunits (IIa and IIb) of unit II are documented between 10 and 16 m. In contrast to unit I, unit II is homogeneous, light grey to grey and clay-rich (cp. Table 1). Calcite minerals are nearly absent, and traces of biological activity as well as pyrite are rare (Fig. S2). The most distinct features of subunit IIa are low S and high MS values. The latter remains high in subunit IIb, while S also increases compared to IIa. PCC values for Ti and Ca for unit II range between −0.3 and 0.7, with the highest values in subunits IIa. The TOC measurements from unit II show values below 2% (Fig. 6).

Unit III

This unit appears between 14.23 and 13.78 m b.s. (IIIa) and between 13.16 and 12.86 m b.s. (IIIb). The upper boundary of IIIa is marked by a distinct erosional unconformity (Fig. 4). Subunit IIIa shows the highest S contents in the core and both subunits are characterised by the lowest Ti/Ca ratios (Figs. 5 and 6). Clastic sediments that dominate unit II are present only as thin laminae. Subunit IIIa is laminated, becoming lighter in colour towards the top, while subunit IIIb is turbated. MS values reach minima in unit III and PCCs for Ti and Ca are at their lowest. Both subunits display distinct minima in EC values (Fig. 6). Smear slides of unit IIIa (Figs. A3 and A4) indicate layers of pyrite, diatom frustules and mineral grains alternating with layers of calcite precipitates.

Unit IV

Unit IV appears in three depth intervals (Fig. 4; Table 1) and clearly differs from under- and overlying units (Figs. 5 and S7). Plant remains and mineral clasts make up the fabric of the sediment, with little to no calcite (Fig. S5). MS values remain low, TOC is elevated and PCC values do not deviate from units I and III. Ti/Ca and EC values peak in unit IV, which is in line with the observation that Ca decreases to very low values.

Unit V

Unit V appears twice in the record (Fig. 4; Table 1), with dark grey to brown silty clay, high TOC content (4%–12%) and low values for gastropods and ostracods. Reed leaves imply the proximity of macrophytes, that is, of the shoreline. While subunit Va shows organic-rich laminae in the lower part and a more homogeneous, dark-brown structure in its upper part, subunit Vb shows a peat-like fabric. Ca minima lead to very high Ti/Ca values. EC data and MS show a distinct decrease coincident with the peat-like subunit Vb (Fig. 6).

Unit VI

The sedimentary sequence terminates with slightly calcareous, rusty greyish–brown silty clay that shows signs of soil formation. The material was compacted by coring and

Figure 4. Photo of sediment core GIA 1A with core numbers (to the right) and lithological units and subunits. Sediment surface: upper left, base of coring: lower right. Large parts of the core are laminated. Frequent changes of the depositional environment are observed in the lower 6 m of the record. (A) Close-up of laminations in unit ib in the upper part of the core. (B) An erosional unconformity is observed at 13.78 m b.s. (red dashed line). [Color figure can be viewed at wileyonlinelibrary.com]

contains roots, while depositional structures are absent. Ti content and MS are increased, while S reaches minima. EC data must be interpreted with caution, as they were measured above the groundwater table (Fischer et al., 2016b).

Chronology

The 11 radiocarbon ages measured for GIA 1A range from 429-295 cal a BP (2 sigma) for the youngest sample to 9396–9022 cal a BP (2 sigma) for the oldest sample (Table 2). A hiatus of c. 1.5 ka is observed between the uppermost two radiocarbon ages, resulting in an average sedimentation rate of 0.12 mm/a f between 1.68 m b.s. and 1.85 m b.s. This coincides with the peat-like subunit Vb described above. The remainder of the record shows a relatively stable average sedimentation rate of 1.6 mm/a. The close spacing of the lowermost radiocarbon dates was chosen to quantify the temporal gap of the erosional discontinuity at 13.78 m b.s., which the age–depth model (Fig. 7) shows to be negligible. The base of the record, at 15.93 m b.s., was extrapolated to represent an age of 10.59 ka BP.

Interpretation and discussion

Geophysical prospecting allowed the identification of an undisturbed location with the thickest sediments (Figs. 2 and 3). The upper unit (A), characterised by low resistivity values, can be interpreted as fine-grained sediments related to a lacustrine depositional environment. This is supported by EC data showing high conductivities from below 2 m to the base of the sequence and by the sedimentary sequence of core GIA 1A (Fig. 4). Layers of coarser grained material, such as lithological unit III, are clearly depicted in EC data but are too thin to be resolved by ERT depth-sections (cp. Fischer et al., 2016b). Unit B, characterised by higher resistivity values, most likely depicts coarser-grained alluvial deposits or reworked Pliocene marl, which lies increasingly close

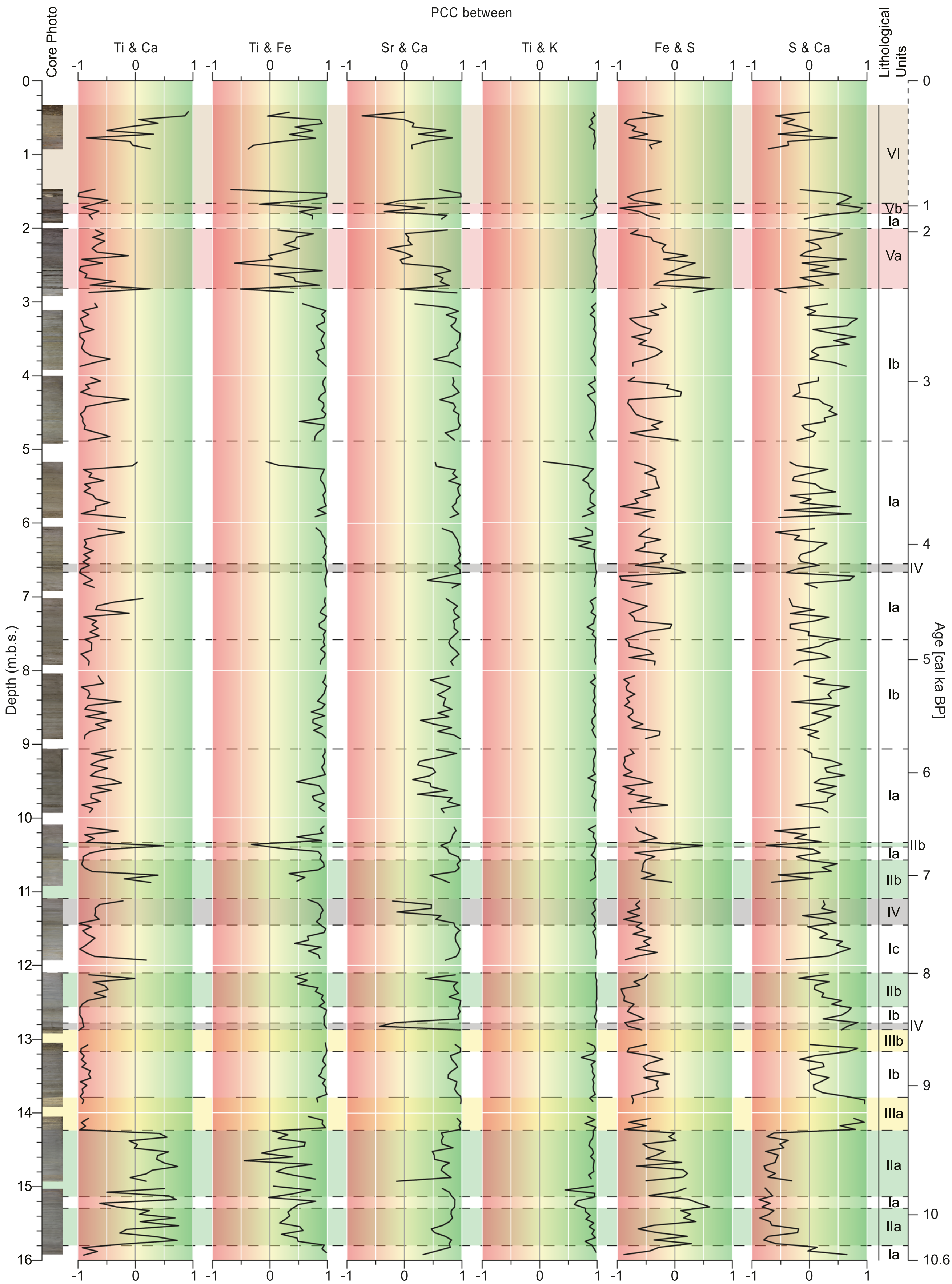

Figure 5. Selected elemental Pearson correlation coefficients (PCC) of sediment core GIA 1A computed for 50 mm sections using high-resolution XRF data, combined with core photos (left) and stratigraphic units (right). Elemental coupling and decoupling can be observed throughout the core. [Color figure can be viewed at wileyonlinelibrary.com]

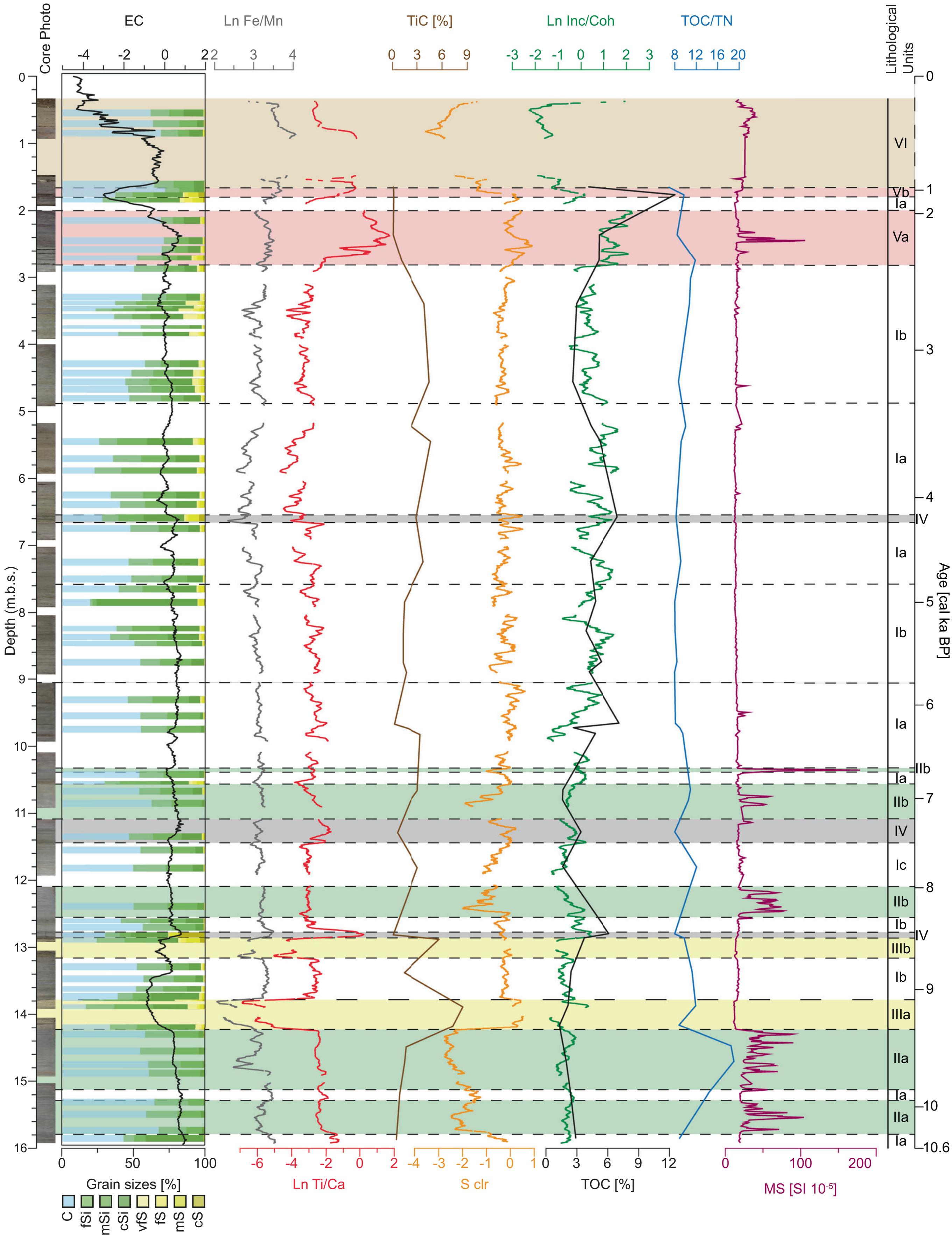

Figure 6. Multiproxy data compiled for the sediment record of GIA 1A. From left to right: Core photo; grain size data and electrical conductivity (EC, normalised, detrended); ln Mn/Fe and ln Ti/Ca smoothed with a 51-point filter; TIC with lower resolution for comparison of selected units; S clr smoothed with a 51-point filter; ln Inc/Coh ratio smoothed with a 51-point filter, overlain with total organic carbon (TOC); TOC/TN; magnetic susceptibility (MS); and lithological units (cf. Table 1). Lithological units are displayed by coloured bars. All data are shown versus depth and calibrated radiocarbon ages (Table 1). [Color figure can be viewed at wileyonlinelibrary.com]

Table 1. Lithological units and subunits for sediment core GIA 1A based on core description.

Lithological unit	Subunit	Depth intervals (m b.s.)	Description
I	a	16.00–15.79 15.29–15.14 10.57–10.40 10.33–9.06 7.58–6.66 6.55–4.88 2.00–1.80	Clayey silt, grey to brownish grey, weakly laminated in some parts, moderately calcareous, molluscs and mollusc fragments, partly with plant/organic remains.
	b	13.78–13.16 12.78–12.56 9.06–7.58 4.88–2.82	Clayey silt, light grey to grey, partly light brown to greenish brown, laminated, moderately calcareous, molluscs and mollusc fragments.
	c	12.10–11.45	Clayey silt, light grey with greyish to light brown, laminated, strongly carbonaceous.
II	a	15.79–15.29 15.14–14.23	Clayey silt, grey to light grey, strongly carbonaceous, homogeneous, weakly laminated in parts, few plant/organic remains.
	b	12.56–12.10 11.09–10.57 10.40–10.33	Clayey silt, light grey to grey, laminated, moderate carbonaceous.
III	a	14.23–13.78	Clayey silt, yellowish beige to light brown, extremely carbonaceous, laminated with dark laminae at the base and light laminae to the top, erosional contact at the top.
	b	13.16–12.86	Clayey silt, beige to light brown, strongly calcareous, numerous molluscs and mollusc fragments.
IV		12.86–12.78 11.45–11.09 6.66–6.55	Clayey silt, grey to dark grey, slightly calcareous, few molluscs, weakly laminated.
V	a	2.82–2.00	Clayey silt, grey to dark grey, lower part laminated with increased (moderate) carbonate content, plant remains in dark laminae, compact towards the top (silting up).
	b	1.80–1.66	Clayey silt, peat-like, dark brown, non-calcareous, decomposed plant remains.
VI		1.66–0.00	Clayey silt, rusty grey to brown, slightly calcareous, stiff, rooted.

Table 2. Radiocarbon dating results of samples collected from GIA 1A.

Sample ID	Lab code	Depth [m b.s.]	Sample material	^{14}C Age	1σ age [cal a BP]	2σ age [cal a BP]
GIA 1A/6 PR 1.66–1.69	45690	1.68	Plant fragment	289 ± 18	423–304	429–295
GIA 1A PR 1,85	56726	1.85	Plant fragment	1935 ± 19	1882–1828	1927–1749
GIA 1A PR 2,20	56727	2.20	Plant fragment	2181 ± 21	2299–2124	2306–2115
GIA 1A/12 PR 2.54	43653	2.54	Plant fragment	2299 ± 20	2348–2327	2353–2184
GIA 1A/25 PR 4.58	43654	4.58	Plant fragment	3030 ± 22	3324–3178	3338–3165
GIA 1A/34 + PR 6.64–6.66	43655	6.65	Plant fragment	3745 ± 22	4150–4015	4225–3989
GIA 1A PR 7,66	56728	7.66	Plant fragment	4304 ± 23	4864–4844	4958–4832
GIA 1A/46 + PR 9.68	43656	9.68	Plant fragment	5497 ± 25	6308–6282	6391–6213
GIA 1A/60 + PR 13.18–13.21	43657	13.20	Plant fragment	8172 ± 27	9131–9026	9266–9016
GIA 1A/63 PR 13.61–13.63	45691	13.62	Plant fragment	8057 ± 26	9020–8813	9081–8780
GIA 1A/66 + PR 14.13–14.15	45692	14.14	Plant fragment	8210 ± 41	9269–9033	9296–9022

to the surface in SE direction (Fig. 3). This is supported by GIA EC 2 and GIA EC 3, both of which show significantly lower EC values (51 mS/m in average) compared to GIA EC 1 (129 mS/m in average).

The geomorphological position at the lowest elevation within the polje at ca. 35 m a.s.l. and the results of ERT and EC measurements clearly imply a lacustrine formation of the underlying sediments, which has been proven by sediment coring. Therefore, the Giannades record is referred to as the Giannades palaeolake in the discussion.

Lacustrine environment and facies interpretation

The lithological units and subunits, along with their detailed geochemical characterisation, allow for a reconstruction of environmental conditions of the Giannades palaeolake.

Unit I makes up most of the record at Giannades Polje. It is therefore interpreted as the equilibrium state of the sedimentary record, to which the system returns after excursions to other states, these being described by the other units; however, the term does not refer to specific geochemical or ecological processes. Although sedimentary features such as lamination and colour vary between subunits Ia and Ic, it is generally characterised by dominance of clay and silt as well as stable geochemical relationships with minor fluctuations (Fig. 6; e.g., MS and TOC/TN). Processes facilitating deposition of Ca and Ti differ, as indicated by their inverse relationship. Fe and Ti maintain a strong positive relationship. Thus, Fe is not altered by secondary processes. Pyrite framboids are present throughout the unit in different concentrations, indicating a reducing environment where Fe and S are bound as FeS. Diatoms are observed in many smear slides (see Figs. S1-S7 for photos of representative smear slides of units), which support the interpretation of a biologically active lake system. Unit I, like all other units of the record, is practically devoid of foraminifera, which strengthens the interpretation that the sediments are of lacustrine origin.

Although unit I often displays laminated sections, these were not analysed in detail because they often occur independently

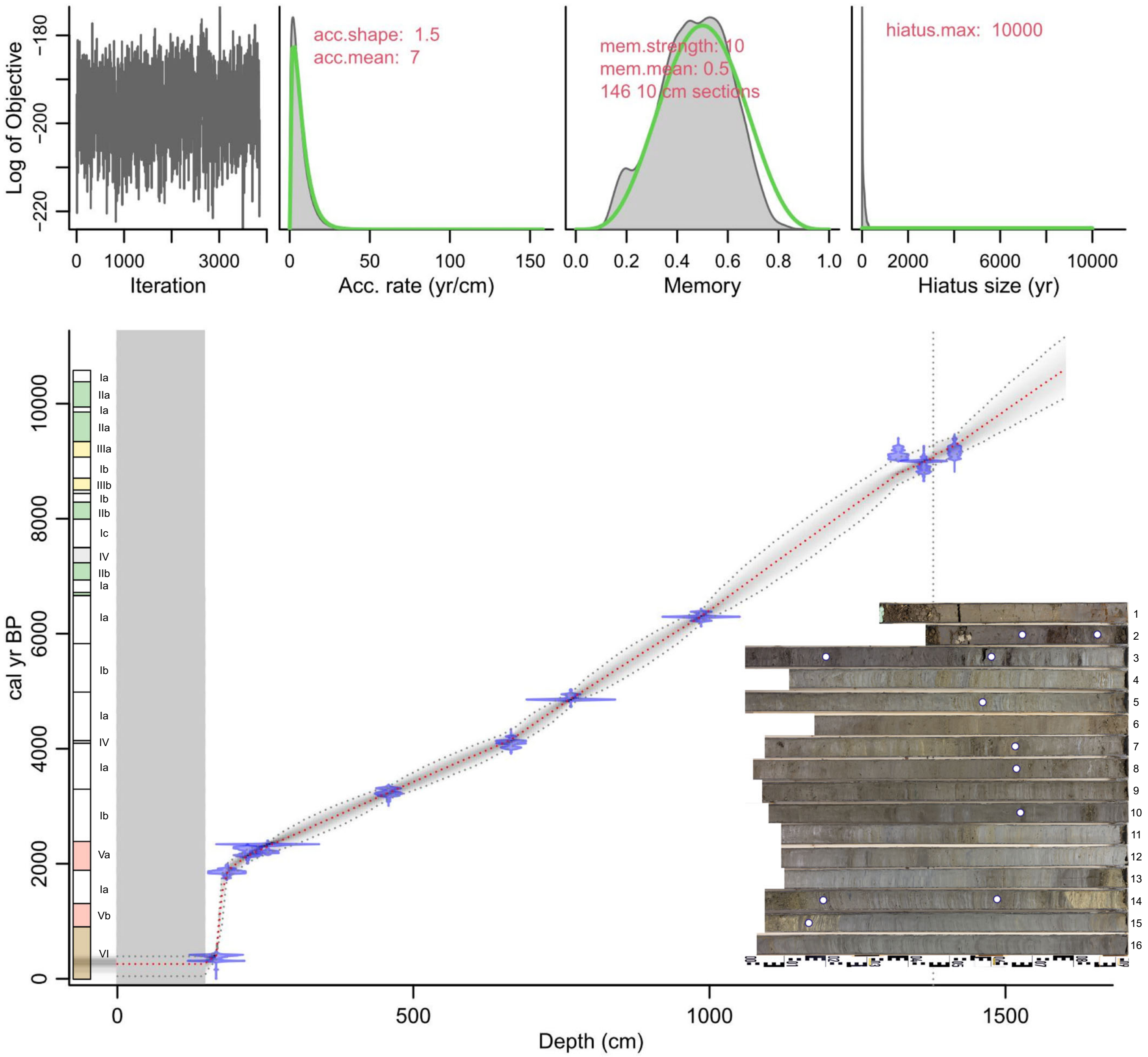

Figure 7. Age–depth model for the sedimentary record of GIA 1A, calculated based on 11 radiocarbon dates obtained from plant remains with the r-package 'rbacon' (Blaauw et al., 2011), using the IntCal20 calibration curve (Reimer et al., 2020). The grey block represents the uppermost core section influenced by anthropogenic impact and soil formation, which is assumed to be modern. The dotted vertical line represents the erosional discontinuity at 13.78 m b.s. Sampling depths are shown in the core photo at the lower right. [Color figure can be viewed at wileyonlinelibrary.com]

of pronounced environmental shifts shown by other parameters. Whether or not a more thorough investigation of these sections with specialised methods can yield valuable insights into past environments remains an open question.

Unit II, which occurs five times below 10.3 m b.s. and before 6.6 cal ka BP, is classified as a unit of **allochthonous dominance under oligotrophic conditions**. This is not necessarily caused by an increase in slope erosion and run-off, but a lack of autochthonous deposition (cp. Fig. S2). Correlations between Ca and Ti are altered compared to the rest of the limnic record, ranging from absent to positive correlations (Fig. 5). This is interpreted as an underlying depositional process, which fits with the observation that the processes usually adding Ca to the sediment are absent, namely, precipitation through alteration of pH through photosynthesis or through evaporation. Possibly, Ca contents are associated with mechanisms related to slope run-off mechanisms that introduce Ti. The lack of calcite precipitation can be interpreted as a decrease in biological productivity. However, low TOC can also be explained by a longer persistence of oxic conditions during summer, enhancing the conditions for microbial decomposition of organic material. The high TOC/TN values might be interpreted as an increased input of terrestrial plant material or as a shift in the ratio of terrestrial to lacustrine production due to reduced within-lake productivity.

MS is the highest in unit II but does not always coincide with increased Fe values. Thus, Fe might partly be present in the form of minerals with comparably high magnetic susceptibility. Fe-bearing minerals may retain their magnetic properties under oxic conditions but reduce to pyrite under anoxic conditions, leading to a decrease in MS (Karlin and Levi, 1983; Cohen, 2003). Thus, the high MS measured in unit II is interpreted as the result of oxic conditions in the hypolimnion, which is supported by scarce observations of pyrite framboids in smear slides (Fig. S2). Mn values are elevated with respect to Fe especially in subunit IIa, which indicates an oxic hypolimnion where Mn is not reduced and remobilized after initial deposition. Moreover, as S seems to be tied to biological productivity in the Giannades lake (weakly positive S and Ca correlation in unit I, strong correlation in unit III), low S concentrations further support the hypothesis of an oligotrophic and oxic environment with minor microbial respiration in the hypolimnion and little precipitation of Ca. However, one would expect a weakened Ti and Fe correlation under anoxic conditions, where the redox-sensitive Fe may undergo secondary changes and detach from the allogenic group. This is not observed in unit IV, which is clearly anoxic. Thus, another explanation for the behaviour of Fe must be found.

Although it is tempting to conclude that allogenic dominance was caused by increased precipitation, it is likely a result of an absence of autogenic deposition and not a sign of increased slope-borne input.

Indeed, some indicators point towards a more arid environment: there is evidence for lower depositional rates when unit II was accumulated (i.e., between 6.2 and 8.8 cal ka BP) compared to phases when unit I dominated (i.e., between 2.3 and 4.2 cal ka BP), indicating no increase in slope run-off. Low TOC values and absent carbonate precipitation indicate a decrease in plant productivity in the lake and on its surrounding slopes. As no increase in run-off is observed from the presumably less overgrown (and thus less erosion-resistant) slopes, it can be concluded that precipitation either remained constant or even decreased. Furthermore, nutrient input is evidently lower in unit II, which could indicate less run-off from the catchment due to less precipitation, or lower temperatures, or both.

Lacey et al. (2015) identified similar conditions of allogenic dominance in Lake Ohrid in the Early Holocene, which terminated 0.6 ka earlier than at Giannades. They favour the interpretation towards cold and arid conditions.

Unit III displays geochemical data (high Ca and low Ln Ti/Ca, high TIC), which indicate the highest **biological activity and calcite precipitation** in the record, along with Ca deposition in the form of shell debris. Detrital material contributes less to unit III, which does not mean that allogenic input was absent. Gastropod shells are rich in this unit and pyrite is abundant in detrital lamina (Fig. S4). Thus, late summer anoxia occurred in individual years, whereas high Mn/Fe values indicate generally oxic environments.

The input of coarse-grained material as expressed by grain-size analysis and minima in EC values are mainly due to shell fragments and calcite crystals. Microscopic analyses at selected depths with high sand contents revealed only very few quartz grains of allogenic origin. This is in line with the core description (Table 1).

The high biological productivity of unit III may be the result of increased temperatures and/or input of nutrients. In the nearby Adriatic Sea, Siani et al. (2013) identified nutrient input via run-off as a driving factor of increased biological activity (Fig. 8).

Subunit IIIa is terminated at 13.78 m b.s. by an erosional unconformity with an angle of ca. 45°. EC data, which were logged some 40 cm distant from the borehole of site GIA 1A, show the end of unit IIIa 38 cm higher compared to the core due to this oblique boundary. However, no high-energy sediments were encountered above the erosional surface. Instead, subunit Ia overlies subunit IIIa.

Subunit IIIb is abruptly terminated at 12.87 m b.s. by the first appearance of **unit IV**, which shows high **eutrophication**, that is, high biological activity with subsequent microbial depletion of oxygen. Unit IV is high in TOC (6% between 12.86 and 12.78 m) and contains very few gastropods and ostracods, clear signs of persistent anoxia (see Fig. S5). Mn has lower values relative to Fe, which indicates that reducing conditions kept Mn from precipitating. Ca values decrease significantly in unit IV because carbonate deposition is inhibited, most likely due to a decrease in pH caused by excessive CO_2 production by microbes, which overcompensates the consumption of CO_2 by photosynthesis (Dean, 1999). The lake record contains several eutrophic phases (represented by unit IV), most pronounced in the subunit between 12.86 and 12.78 m b.s. The other occurrences of unit IV further up core (11.45–11.09 and 6.66–6.55 m b.s.) show less pronounced characteristics of eutrophication compared to the subunit between 12.86 and 12.78 m b.s.: some carbon precipitation persists, and TOC values are not as elevated.

Unit V is similar to unit IV in appearance (see Fig. S6), but the key differences outlined in section 4.1. (macrophyte presence, peat-like appearance of subunit Vb) are interpreted as **progressive desiccation**. Precipitation of Ca has ceased, which is reflected by minimum values, and TOC is elevated, especially in subunit Vb, where it reaches >12%; this fits with the macroscopic identification of organic matter. Desiccation occurred in two phases, expressed by a short-term return to limnic conditions in subunit Ia between 2.00 and 1.80 m b.s., where faint laminations are visible and carbonate precipitation occurred before the lake finally silted up. According to the chronology, the subsequent wetland phase lasted for over one millennium. However, it cannot be excluded that roots contaminated the youngest radiocarbon age, causing a large temporal gap.

Unit V is likely dominated by processes governed by local geomorphology, but climate impacts may have been a driver of the first period of desiccation, and drainage by humans cannot be ruled out.

After desiccation of the lake, **unit VI**, consisting of **pedogenically altered sediments** without discernible depositional structures, terminates the sedimentary sequence. As the site has been used for agricultural purposes for a long time, sediments must be considered disturbed. Therefore, further analysis, interpretation and discussion will focus on units I–V.

Palaeo-hydrological interpretation

The Giannades record is sensitive to both climate changes and seismotectonic events and can be divided into three periods: (i) A highly variable lake environment during the Early and Mid-Holocene between 10.6 and 6.6 cal ka BP with frequent changes of environmental conditions, most likely related to RCCs; (ii) a Mid- to Late Holocene stabilisation of the lake system for over four millennia (6.6–2.3 cal ka BP); and (iii) desiccation, which terminates the lake record after 2.3 cal ka BP (Fig. 8).

The palaeoenvironmental variability in the Giannades sedimentary record increased during the Early Holocene until 6.6 cal ka BP. This either indicates a Mid-Holocene decrease in climate variability translating into the sedimentary record, or the lake system stabilised after a period of increased Early Holocene hydrological variability.

Some regional records, like Lake Butrint in Albania (Morellón et al., 2016), less than 30 km from Giannades Polje, show varying climate sensitivity due to a shifting dominance of climatic, geomorphological, anthropogenic and seismic forcings (Morellón et al., 2016; see also Haenssler et al., 2013 for the Lagoon of Etoliko; Seguin et al., 2019 for Lake Stymphalia). It also must be considered that large parts of the NW mainland of Greece and the NW Peloponnese have been subject to repeated regional (seismo-) tectonic events since the Mid-Holocene (around 6000, 4500, 2500 and 2250, 1750 and 750 cal BP; see, e.g., Vött, 2007), which have controlled the sea-level evolution by tectonically induced changes in land elevation. It may be assumed that similar

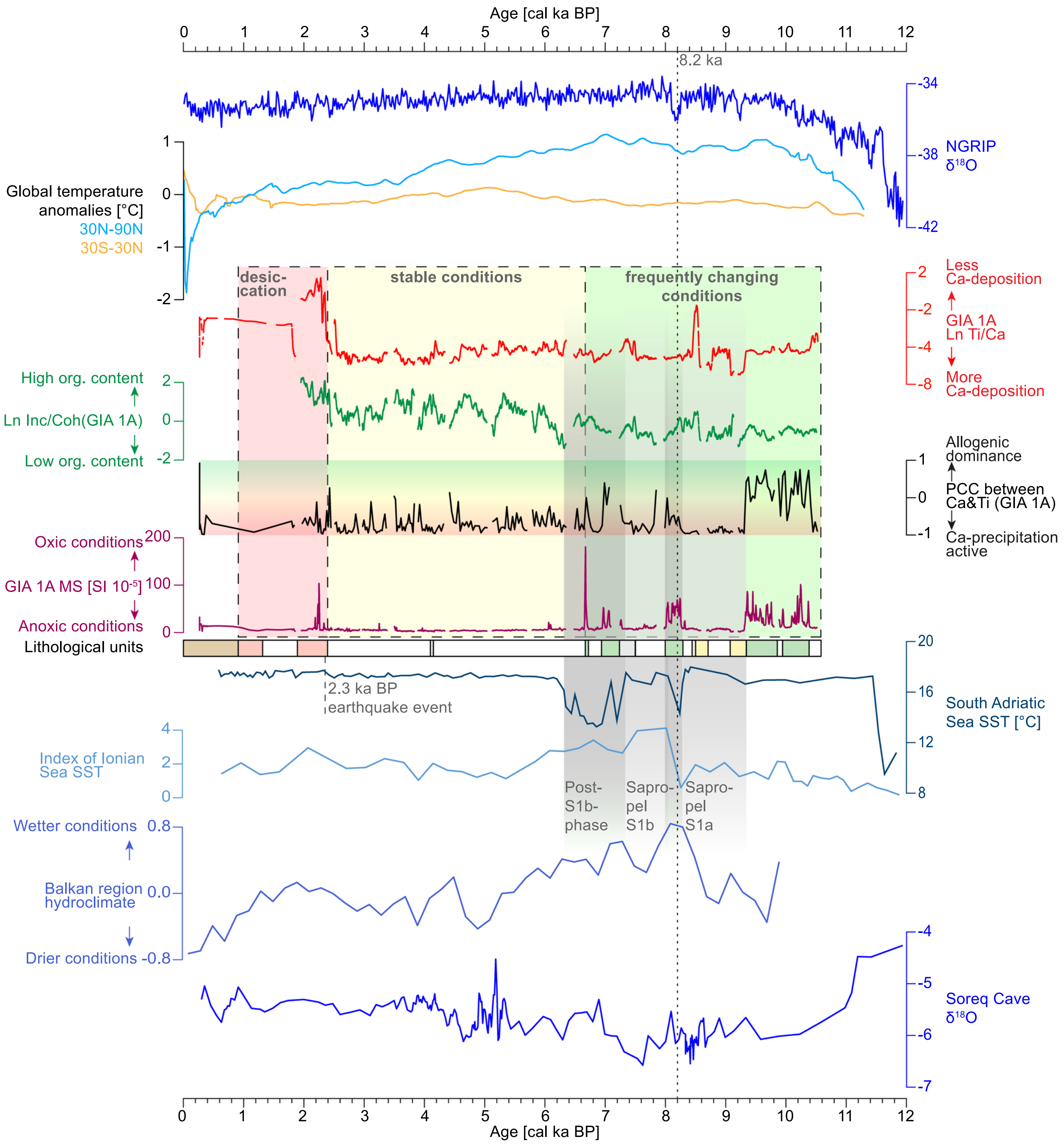

Figure 8. Comparison of the Giannades sedimentary record GIA 1A with regional and supra-regional archives and palaeoenvironmental reconstructions (cp. Fig. 1). From top to bottom: NGRIP $\delta^{18}O$ record (Rasmussen et al., 2006); global temperature anomalies for 30S–30N and 30N-90N compiled by Marcott et al. (2013); GIA 1A Ln Ti/Ca ratio as a proxy for carbonate deposition; GIA 1A Ln incoherent/coherent ratio as a proxy for organic matter; PCC between Ca and Ti (50 mm segments) as a proxy for carbonate origin; MS as a proxy for oxic/anoxic conditions; MD90-917 South Adriatic Sea sea surface temperatures (SST) record (Siani et al., 2013); Z1 Ionian Sea SST index (Geraga et al., 2008); multi-proxy hydroclimate reconstruction of the Balkan region at 0.2-ka resolution (Finné et al., 2019); and speleothem $\delta^{18}O$ record from Soreq cave, Israel (Bar-Matthews et al., 2003). Sapropel deposition is marked with grey bars after Siani et al. (2013). The vertical dotted line marks the 8.2 ka event. [Color figure can be viewed at wileyonlinelibrary.com]

events also occurred earlier and might have been imprinted into palaeoenvironmental records by seismotectonic forcing throughout the entire Holocene.

High environmental variability between 10.6 and 6.6 cal ka BP

Arid environmental conditions were observed in the oldest sections of the Giannades lake record (10.6–9.3 cal ka BP) after the onset of the Holocene. There is ample evidence for nutrient shortage and persistent oxygenation under oligotrophic conditions, which are characteristic of cold and dry climatic conditions (unit II). Comparable conditions are reported from other regional archives, like Lake Prespa (Kotthoff et al., 2008; Cvetkoska et al., 2014) and the multi-proxy synthesis of Finné et al. (2019). Emmanouilidis et al. (2020), however, report on perennial humid conditions at Lake Vouliagmeni for the period

10.8–8.0 cal ka BP. This discrepancy is potentially explained by the location of Lake Vouliagmeni in the Eastern Gulf of Corinth, separated from Giannades Polje by 320 km and the Pindus and Peloponnese mountain ranges. If the cooling is caused by cold and arid air masses coming from the North, these will reach Giannades Polje without having passed over significant water bodies and remain arid, but they will reach Lake Vouliagmeni after having passed over the Aegean Sea, where these arid air masses can take up water. This highlights the climatic heterogeneity of the Mediterranean region, and the resulting need to investigate a large number of sites.

The sudden shift at 9.3 cal ka BP towards highly productive conditions with high carbonate precipitation coincides with the onset of sapropel S1 in the South Adriatic Sea (Siani et al., 2013). This timing, however, is later than the 9.9-ka transition observed by Geraga et al. (2008) in the Ionian Sea and the 9.5-ka transition reported for the Aegean Sea by Kotthoff et al. (2008). Siani et al. (2013) observe a slight freshening of the South Adriatic Sea salinity during this time, indicating a shift from arid conditions to more humid conditions. The onset of Sapropel S1 is linked to an orbitally forced African monsoon intensification, which facilitated increased freshwater and nutrient input into the Eastern Mediterranean Sea via the Nile River and its tributaries but also created wetter conditions as far as the southern Adriatic Sea (Siani et al., 2013), which lies close to Giannades Polje. These wetter conditions may have caused increased run-off and nutrient supply at the Giannades palaeolake, which is in line with the observations in sediment core GIA 1A. The period of very high productivity is capped by the first appearance of unit IV, a phase with a high nutrient supply compared to the rest of the record.

Between 8.3 and 8.0 cal ka BP, cold and arid conditions comparable to those observed prior to 9.3 ka BP returned to Giannades. Distinct cold spells around this time are commonly associated with the 8.2-ka event. This is represented in Greenland ice cores as a negative excursion in the $\delta^{18}O$ values and was caused by a large glacial meltwater discharge into the North Atlantic that weakened the thermohaline circulation and led to a short (<200 a) period of atmospheric cooling (Thomas et al., 2007). The 8.2-ka event is found in many climate archives throughout the northern hemisphere (see the global temperature anomaly record by Marcott et al. (2013; Fig. 8) and most clearly present in archives impacted by Atlantic circulation patterns (Thomas et al., 2007). However, some authors assign multi-centennial cold spells in their archives to the short 8.2 ka event despite chronological uncertainties and a likely superposition of both the short 8.2 ka event and a multi-centennial RCC (Rohling and Pälike, 2005; Thomas et al., 2007; Rohling et al., 2019). The cold and arid signal is common in many Mediterranean archives, for example, Lake Ohrid (Lacey et al., 2015). In Lake Djoran, low lake levels and increased allogenic supply are interpreted by Francke et al. (2013) as cold and dry conditions in combination with reduced vegetation cover. Avramidis et al. (2013) identified cold and arid conditions in Zakynthos Island for the period 8.3–8.1 ka BP based on pollen assemblages.

The cold and arid signal observed at Giannades is coincident with the interruption of sapropel S1 in marine archives by a distinct cold phase at around 8.2 ka BP, which is recorded by 3°C lower SSTs in the Adriatic Sea and a similar cooling in the Ionian Sea (Geraga et al., 2008; Siani et al., 2013). In the Aegean Sea, this S1 interruption was observed by Kotthoff et al. (2008) between 8.4 ka BP and 8.0 ka BP. This interruption is only found in the Northern Mediterranean affected by Atlantic or continental air masses and absent in the Eastern Mediterranean (Rohling et al., 2015).

On Corfu, Berger et al. (2016) found evidence for increased erosion and fluvial activity associated with the 8.2 ka event at Sidari, a small coastal valley, approx. 20 km NW of the Giannades palaeolake. They interpret their findings as hydrological changes in the catchment instead of generally wetter conditions. According to Berger et al. (2016), snow cover at higher elevations enabled by colder conditions may have caused spring meltwater floods, and summer rain may have increased while evapotranspiration decreased.

Finné et al. (2019) provide hydroclimate proxies for the period from 10 ka until present, and the highest precipitation given by their multi-proxy Z-score synthesis for the Balkan region (Fig. 8) is reported for the period 8.2–8.0 ka. Only six records cover the time frame in question, for example, the Lake Djoran sedimentary record (Francke et al., 2013) and the Lake Ohrid record (Lacey et al., 2015). Whereas Francke et al. (2013) contextualise their findings of increased K and Fe with a likely reduction of vegetation cover leading to increased detrital input despite more arid conditions, the Z-score synthesis uses the K-proxy to indicate high precipitation without considering this limitation. The same is true for the sedimentary record of Lake Ohrid, where a complex qualitative interpretation by Lacey et al. (2015) describes arid conditions, but the K-proxy used by Finné et al. (2019), taken out of this context, implies wet conditions. The Z-score record of Lake Ohrid contributes the largest supposed precipitation signal to the synthesis, which incorrectly skews the synthesis towards wetter conditions. The synthesis by Finné et al. (2019) provides valuable information on long-term hydroclimatic trends. However, individual peaks and minima must be interpreted with caution, as they might be caused by overgeneralizing.

After the 300-year excursion towards cold and dry conditions, biological productivity increased again in the Giannades palaeolake, although it was less pronounced than before. From 7.5 to 7.3 cal ka BP, another eutrophic phase occurred, reflected by the second appearance of unit IV between 11.45 and 11.09 m b.s. The period between 8.0 and 7.3 cal ka BP is temporally closely aligned with the deposition of sapropel S1b in the Adriatic Sea (Siani et al., 2013; see also Avramidis et al., 2013), which resumed after the interruption centred around 8.2 ka.

From 7.3 to 6.6 cal ka BP, the last oligotrophic phase under cold and arid conditions occurred within subunit IIb. This is remarkably in phase with the South Adriatic Sea post-sapropel cooling with decreasing SSTs of as much as 4°C reported for 7.3–6.3 ka BP by Siani et al. (2013). Rohling et al. (2015) and Siani et al. (2013) attribute the impact of RCCs in the form of a centennial influx of cold continental air masses during wintertime as the cause for these lower SST. Moreover, Siani et al. (2013) document that sapropel S1 terminated because of deep-water oxygenation caused by the creation of denser surface waters. Given the thermal stability of water, we assume that the same air masses that lowered the South Adriatic SSTs by 4°C also caused the observed oligotrophic conditions at Giannades. Corroborating data are reported by Emmanouilidis et al. (2020) from Lake Vouliagmeni, who used geochemical proxies, and Avramidis et al. (2013) for the Ionian Islands, who used pollen data.

Period of relative stability from 6.6 to 2.3 cal ka BP

Between 6.6 and 2.3 cal ka BP, the sediments of the Giannades palaeolake show remarkable stability after four millennia of frequent environmental changes. This agrees with other regional lake records, which document gradual trends towards a drier climate (Zanchetta et al., 2007; Leng et al., 2010; Francke et al., 2013; Lacey et al., 2015; Finné et al., 2019). While the GIA 1A record remains visually variable and many elemental curves continue to show excursions, no clear shifts to different environmental states of the lake system are evident, except for one eutrophic phase from 4.4 to 4.2 ka BP (unit IV between 6.66 and 6.55 m b.s.). Here, unit IV is less pronounced than its previous iterations but is still characterised by high OC contents and decreased Ca, indicating a shift to more nutrient-rich conditions. This can be interpreted as an increased nutrient supply by wetter conditions, but the coincidence with the 4.2 ka BP cooling event that some authors associate with dry conditions is in contrast with this interpretation (Francke et al., 2013). In a synthesis of Mediterranean records with a focus on the 4.2 ka BP event, Bini et al. (2019) identify contradicting climate signals in regional records and conclude that current data are insufficient to create a coherent synthesis.

The desiccation phase after 2.3 cal ka BP—seismic, anthropogenic or climatic?

To understand the desiccation of the Giannades palaeolake, the gap in the Pliocene flysch ridge (Fig. 2(C)), which separates the polje from the Ionian Sea, needs to be considered as the limit for the maximum lake level. Any changes of the gap directly impacted the lake. The fact that the lake recovered for a brief period of limnic conditions (2.0–1.8 ka BP) after the desiccation at 2.3 cal ka BP and resumed desiccation again at 1.8 cal ka BP indicates a more complex interpretation than gradual sedimentation until the lake basin is filled up.

The onset of unit Va around 2.3 cal ka BP, which represents a desiccation process, coincides with a local seismic uplift event identified by Finkler et al., (2018b, 2019) for the fourth/third century BC. During this earthquake, the west coast of Corfu was uplifted more than the east coast, resulting in a tilting of the northern part of the island (Finkler et al., 2018b). This earthquake also caused the destruction of the famous Temple of Hera in ancient Kerkyra (Finkler et al., 2018b) and was associated with a tsunami, traces of which have been encountered in coastal archives of Corfu (Finkler et al., 2019). It further led to the abandonment of the Pierri harbour at the east coast of Corfu, while the Desylla and Kokotou harbour basins subsequently had to be cleaned from tsunami deposits (Finkler et al., 2018b, 2019).

The same tectonic event is corroborated by data derived from palaeo-sea-level markers in coastal rocks from Mastronuzzi et al. (2014) and Evelpidou and Pirazzoli (2014). Therefore, three possible effects of this seismotectonic event have to considered with regard to the Giannades proxy data: (i) at a time of high lake levels, seismic disturbance of the narrow gap damming the lake may have caused a partial collapse of this dam, lowering the lake level abruptly; (ii) tilting of the island may have raised the outflow level of the lake during the process of desiccation and caused a temporary return to lacustrine conditions; or (iii) subsurface water pathways in the local karstic hydrological system may have been activated, lowering the lake level.

Repeated filling and emptying of a lake in a comparable environmental setting (Pheneos polje, northern Peloponnese) have been associated with activation and/or de-activation of underground karst hydrological pathways by strong earthquakes since ancient times (Clark, 1858; Hasluck, 1937; Philippson, 1959; Grove and Rackham, 2001; Clendenon, 2010; for more details and references see Vött, 2013). In the context of an earthquake event that hit northern Corfu at 2.3 cal ka BP, a plausible interpretation is the activation of subsurface water pathways that temporarily drained the lake.

Furthermore, human activity in the polje may have increased desiccation. Inhabitants of Corfu may have realised that manipulation of the gap can help to easily drain parts of the lake to create arable land. While there is no direct evidence of human activity in the Giannades record, it must be considered as a plausible factor. Haenssler et al. (2013) observed effects of human impact on the catchment of Etoliko Lagoon during the late Bronze Age (3.65–3.05 cal ka BP). Emmanouilidis et al. (2022) assign a sudden increase in sedimentation in Lake Vouliagmeni after 3.0 cal ka BP to human activity. Lespez (2003) found that Mediterranean landscapes were especially strongly altered between 2.3 and 1.3 ka.

Climatic drivers must also be considered. An arid phase that shifts the balance between precipitation and evaporation potentially can accelerate desiccation of a shallow lake. Due to sediment infilling, the lake is unlikely to have been deeper than 3 m at the study site when desiccation set in, which makes it susceptible to water-level fluctuations with desiccation. It is possible that the Giannades palaeolake experienced an increase in summer evaporation relative to winter precipitation between 2.3 and 2.0 cal ka BP and desiccation set in, but wetter conditions around 2.0 cal ka BP replenished the lake water until 1.8 cal ka BP. Morellón et al. (2016) suggested that similar conditions occurred in lake Butrint, Albania, at the same time. However, it is likely that the strong earthquake that hit northern Corfu in the fourth/third century BCE (2.3 cal ka BP, Finkler et al., 2018b, 2019) also affected adjacent Albania and Lake Butrint, suggesting seismic or tsunami-related forcing as potential drivers.

Morellón et al. (2016) report a decrease in salinity starting at 1.95 ka in lake Butrint and interpret this as the onset of warm and wet conditions. Regional archives generally report a warm and dry climate for the Roman Warm Period (RWP), which is generally stated to span ca. 2.0–1.8 ka BP (Manning, 2013; Finné et al., 2011). Francke et al. (2013) report lower lake levels and anoxic conditions facilitating reed beds at Lake Djoran for this period, which is in line with observations at Giannades. Lacey et al. (2015) document increasingly wet conditions that began around 2.0 ka at Lake Ohrid. Therefore, also climatic conditions correlate with the onset (2.3 cal ka BP) and subsequent pause (2.0–1.8 cal ka BP) of desiccation at the Giannades palaeolake.

Between 2.3 and 1.8 cal ka BP, the lake was shallow and sensitive to various possible triggers of desiccation, such as the simultaneous occurrence of a strong seismo-tectonic event and the existence of a climatic trend related to the RWP, but none of these hypotheses is strongly supported in comparison to the others. Similar difficulties in assigning tectonic, climatic or anthropogenic drivers to a complex lake desiccation process are reported by Katrantsiotis et al. (2015). However, the coincidence of the onset of desiccation at Giannades with a strong local earthquake and tectonic effects such as uplifting and tilting of the island, plus a tsunami landfall causing destruction of buildings and harbours, is striking and suggests at least some role for tectonics. Most probably, proxy changes observed in Mediterranean karst regions cannot *a priori* be related to climatic drivers but may have multiple origins.

Conclusions

The palaeolake record from Giannades on Corfu, Greece, has high potential to provide palaeoenvironmental information. Spanning at least 10.6 cal ka BP, the near-continuous and high-resolution record shows a sensitivity to Holocene RCCs and, especially in the late Holocene, to seismotectonic and anthropogenic impacts.

- During the Early to Mid-Holocene (10.6–6.6 cal ka BP), the lake shows a high sensitivity to hydroclimatic changes with alternating climate conditions. An oligotrophic environment

indicative of cold and arid conditions from 10.6 until 9.3 cal ka BP is followed by a warm and wet period with a highly productive lake until 8.3 cal ka BP, which coincides with the deposition of sapropel S1a in the South Adriatic Sea. From 8.3 to 8.0 cal ka BP, cold and arid conditions returned, a process in phase with widespread observations of the supra-regional 8.2 ka event. From 8.0 to 7.3 cal ka BP, warm and wet conditions continue corresponding to sapropel S1b, and between 7.3 and 6.6 cal ka BP, cooling re-established another oligotrophic period.
- From 6.6 until 2.3 ka BP, the Giannades palaeolake shows stable ecological conditions, which is similar to the behaviour of other regional lakes.
- The onset of desiccation at 2.3 cal ka BP coincides with a well-documented regional seismo-tectonic event, possibly changing the karst-hydrological and geomorphological settings towards draining of the lake. Desiccation continued during the RWP with more arid conditions, possibly facilitating lower lake levels through increased evaporation. Drainage measures to create arable land are not supported by evidence, but may nonetheless have contributed to desiccation in this interval.

In summary, the Giannades sedimentary record is a valuable palaeoclimatic archive for the Mediterranean region, demonstrating temporal correlations with other regional archives. A picture is emerging of a region with high sensitivity to rapid climate changes, a pattern that is well demonstrated by the high-resolution multiproxy data at Giannades. Corfu's location at the boundary between the subtropical high and the temperate climate system of Central Europe makes it potentially sensitive to RCCs caused by centennial-scale switches to the influx of wintertime cold air, and this dynamic strongly characterised the earlier part of the Holocene. Records from locations such as Giannades may be complicated by the effects of seismotectonic events, underlining the need to compare records with different sensitivities to these events in order to identify more recent climate dynamics. Nevertheless, the Roman and post-Roman periods in Corfu and the eastern Mediterranean likely saw an overall trend towards increasing aridity.

Acknowledgements. We thank all involved members of the Natural Hazard Research and Geoarchaeology team and of the Soil Geography group at Mainz, especially Gerlinde Borngässer and Stefanie Klassen, for their help during laboratory analyses. This research is part of the project entitled 'Extreme events in the Holocene geological record of Corfu (Ionian Islands, Greece) and their influence on man and environment' (German Research Foundation, DFG, project number 280180719). It is also embedded in the multidisciplinary GroundCheck programme of the Deutsches Archäologisches Institut, project 'Caves and Lakes—Speleothems and lake sediments in Greece'. Open Access funding enabled and organized by Projekt DEAL.

Data Availability Statement

All basic data will be accessible via the central project server of Johannes Gutenberg-Universität Mainz in cooperation with the Center for Data Processing at JGU using the following link: https://seafile.rlp.net/d/684e0a967b4e477098f1/.

Supporting information

Additional supporting information can be found in the online version of this article.

Table S1. Core recovery rate. The lowermost 7 cm of each core were recovered from the core head in sampling bags.

Figure S1. Smear slide of unit I (5.43 m b.s.) showing mineral grains, shell debris, diatom frustules, plant matter, some pyrite and sponge spicules. Abundance of constituents varies throughout the unit.

Figure S2. Smear slide of unit II (14.79 m b.s.) consisting mainly of clay-sized particles originating from the catchment slopes. Ca deposition and burial is nearly absent, pyrite is rare.

Figure S3. Smear slide of unit III (14.190 m b.s.) showing that one of two main constituents of unit III is calcite precipitation (during summer).

Figure S4. Smear slide of unit III (14.195 m b.s.) shows pyrite, diatom frustules and mineral grains representing main constituents of sedimentary input during winter.

Figure S5. Smear slide of unit IV (12.80 m b.s.) without Ca deposition.

Figure S6. Smear slide of unit V (2.16 m b.s.) shows similarities to unit IV but documents the desiccation state of the lake.

Figure S7. Elemental composition along sediment core GIA 1A combined with core photos (left) and lithological units (right). Elemental records are clr-transformed, normalized to zero mean and unit standard deviation to remove dilution effects and enable statistical analyses, and are shown with their original resolution (1 mm, in grey) and with a 51-point running average (red/black) to visualize trends (see text for further explanations).

References

Avramidis, P., Geraga, M., Lazarova, M. & Kontopoulos, N. (2013) Holocene record of environmental changes and palaeoclimatic implications in Alykes Lagoon, Zakynthos Island, western Greece, Mediterranean Sea. *Quaternary International*, 293, 184–195.

Bar-Matthews, M., Ayalon, A., Gilmour, M., Matthews, A. & Hawkesworth, C.J. (2003) Sea–land oxygen isotopic relationships from planktonic foraminifera and speleothems in the Eastern Mediterranean region and their implication for paleorainfall during interglacial intervals. *Geochimica et Cosmochimica Acta, A Special Issue Dedicated to Robert Clayton,* 67, 3181–3199. https://doi.org/10.1016/S0016-7037(02)01031-1

Berger, J.-F. & Guilaine, J. (2009) The 8200 cal BP abrupt environmental change and the Neolithic transition: a Mediterranean perspective. *Quaternary International*, 200(1–2), 31–49.

Berger, J.-F., Lespez, L., Kuzucuoğlu, C., Glais, A., Hourani, F., Barra, A. et al. (2016) Interactions between climate change and human activities during the early to mid-Holocene in the eastern Mediterranean basins. *Climate of the Past*, 12(9), 1847–1877.

Bertrand, S., Tjallingii, R., Kylander, M.E., Wilhelm, B., Roberts, S.J., Arnaud, F. et al. (2024) Inorganic geochemistry of lake sediments: a review of analytical techniques and guidelines for data interpretation. *Earth-Science Reviews*, 249, 104639.

Bini, M., Zanchetta, G., Perşoiu, A., Cartier, R., Català, A., Cacho, I. et al. (2019) The 4.2 ka BP event in the Mediterranean region: an overview. *Climate of the Past*, 15, 555–577.

Blaauw, M. & Christen, J.A. (2011) Flexible paleoclimate age-depth models using an autoregressive gamma process. *Bayesian Analysis*, 6(3), 457–474.

Clark, W.G. (1858) *Peloponnesus: notes of study and travel*. London: Parker and Son.

Clendenon, C. (2010) Ancient Greek geographer Pausanias as a qualitative karst hydrogeologist. *Ground Water*, 48(3), 465–470.

Cohen, A.S. (2003) *Paleolimnology. The history and evolution of lake systems*. New York: Oxford.

Cvetkoska, A., Levkov, Z., Reed, J.M. & Wagner, B. (2014) Late Glacial to Holocene climate change and human impact in the Mediterranean: the last ca. 17ka diatom record of Lake Prespa (Macedonia/Albania/Greece). *Palaeogeography, Palaeoclimatology, Palaeoecology*, 406, 22–32.

Dean, W.E. (1999) The carbon cycle and biogeochemical dynamics in lake sediments. *Journal of Paleolimnology*, 21(4), 375–393.

Emmanouilidis, A., Katrantsiotis, C., Dotsika, E., Kokkalas, S., Unkel, I. & Avramidis, P. (2022) Holocene paleoclimate variability in the eastern Mediterranean, inferred from the multi-proxy record of Lake Vouliagmeni, Greece. *Palaeogeography, Palaeoclimatology, Palaeoecology*, 595, 110964.

Emmanouilidis, A., Unkel, I., Seguin, J., Keklikoglou, K., Gianni, E. & Avramidis, P. (2020) Application of non-destructive techniques on a varve sediment record from Vouliagmeni Coastal Lake, Eastern Gulf of Corinth, Greece. *Applied Sciences*, 10(22), 8273.

Evelpidou, N. & Pirazzoli, P.A. (2014) Holocene relative sea-level changes from submerged tidal notches: a methodological approach. *Quaternaire*, 25(4), 313–320.

Ferentinos, G., Gkioni, M., Geraga, M. & Papatheodorou, G. (2012) Early seafaring activity in the southern Ionian Islands, Mediterranean Sea. *Journal of Archaeological Science*, 39(7), 2167–2176.

Finkler, C., Baika, K., Rigakou, D., Metallinou, G., Fischer, P., Hadler, H. et al. (2018a) Geoarchaeological investigations of a prominent quay wall in ancient Corcyra—implications for harbour development, palaeoenvironmental changes and tectonic geomorphology of Corfu Island (Ionian Islands, Greece). *Quaternary International*, 473, 91–111.

Finkler, C., Baika, K., Rigakou, D., Metallinou, G., Fischer, P., Hadler, H. et al. (2019) The sedimentary record of the Alkinoos Harbour of ancient Corcyra (Corfu Island, Greece)— geoarchaeological evidence for rapid coastal changes induced by co-seismic uplift, tsunami inundation and human interventions. *Zeitschrift für Geomorphologie, Supplementary Issues*, 62(2), 197–246. Available from: https://doi.org/10.1127/zfg_suppl/2018/0514

Finkler, C., Fischer, P., Baika, K., Rigakou, D., Metallinou, G., Hadler, H. et al. (2018b) Tracing the Alkinoos Harbor of ancient Kerkyra, Greece, and reconstructing its pale-otsunami history. *Geoarchaeology*, 33(1), 24–42. Available from: https://doi.org/10.1002/gea.21609

Finné, M., Holmgren, K., Sundqvist, H.S., Weiberg, E. & Lindblom, M. (2011) Climate in the eastern Mediterranean, and adjacent regions, during the past 6000 years—A review. *Journal of Archaeological Science*, 38(12), 3153–3173.

Finné, M., Woodbridge, J., Labuhn, I. & Roberts, C.N. (2019) Holocene hydro-climatic variability in the Mediterranean: a synthetic multi-proxy reconstruction. *The Holocene*, 29(5), 847–863.

Fischer, P., Finkler, C., Röbke, B.R., Baika, K., Hadler, H., Willershäuser, T. et al. (2016a) Impact of Holocene tsunamis detected in lagoonal environments on Corfu (Ionian Islands, Greece)—geomorphological, sedimentary and microfaunal evidence. *Quaternary International*, 401, 4–16. Available from: https://doi.org/10.1016/j.quaint.2015.07.019

Fischer, P., Wunderlich, T., Rabbel, W., Vött, A., Willershäuser, T. & Baika, K. et al. (2016b) Combined electrical resistivity tomography (ERT), direct-push electrical conductivity (DP-EC) logging and coring—a new methodological approach in geoarchaeological research. *Archaeological Prospection*, 23(3), 213–228.

Francke, A., Wagner, B., Leng, M.J. & Rethemeyer, J. (2013) A Late Glacial to Holocene record of environmental change from Lake Dojran (Macedonia, Greece). *Climate of the Past*, 9(1), 481–498.

Frogley, M.R., Griffiths, H.I. & Heaton, T.H.E. (2001) Historical biogeography and Late Quaternary environmental change of Lake Pamvotis, Ioannina (north-western Greece): evidence from ostracods. *Journal of Biogeography*, 28(6), 745–756.

Geraga, M., Mylona, G., Tsaila-Monopoli, S., Papatheodorou, G. & Ferentinos, G. (2008) Northeastern Ionian Sea: palaeoceanographic variability over the last 22 ka. *Journal of Marine Systems*, 74(1–2), 623–638.

Grove, A.T. & Rackham, O. (2001) *The nature of Mediterranean Europe. An ecological history*. New Haven/London: Yale University Press. p. 384.

Haenssler, E., Nadeau, M.-J., Vött, A. & Unkel, I. (2013) Natural and human induced environmental changes preserved in a Holocene sediment sequence from the Etoliko Lagoon, Greece: new evidence from geochemical proxies. *Quaternary International*, 308–309, 89–104.

Hasluck, M. (1937) Causes of the fluctuations in level of Lake Ostrovo, West Macedonia. *The Geographical Journal*, 90(5), 446–457.

IGME. (1970) *Geological Map of Greece. Sheet North and South Corfu*. 1:50,000. Athens: Institute of Geology and Mineral Exploration (IGME).

Jahn, R., Blume, H.P., Asio, V.B., Spaargaren, O. & Schad, P. (2006) *Guidelines for soil description*, 4th edition. Rome: Food and Agriculture Organization of The United Nations (FAO).

Jahns, S. (2005) The Holocene history of vegetation and settlement at the coastal site of Lake Voulkaria in Acarnania, western Greece. *Vegetation History and Archaeobotany*, 14(1), 55–66.

Karlin, R. & Levi, S. (1983) Diagenesis of magnetic minerals in recent haemipelagic sediments. *Nature*, 303(5915), 327–330.

Katrantsiotis, C., Norström, E., Holmgren, K., Risberg, J. & Skelton, A. (2015) High-resolution environmental reconstruction in SW Peloponnese, Greece, covering the last c. 6000 years: evidence from Agios Floros fen, Messenian plain. *The Holocene*, 26(2), 188–204.

Kiechle, F.K. (1979) Korkyra und der Handelsweg durch das Adriatische Meer im 5. Jh. v. Chr. *Zeitschrift für Alte Geschichte*, 28(2), 173–191.

Köhn, M. (1929) Korngrößenbestimmung mittels Pipettanalyse. *Tonindustriezeitung*, 55, 729–731.

Kokkalas, S., Xypolias, P., Koukouvelas, I. & Doutsos, T. (2006) Postcollisional contractional and extensional deformation in the Aegean region. In: Dilek, Y. & Pavlides, S. (Eds.) *Postcollisional tectonics and magmatism in the Mediterranean region and Asia*. Boulder, CO: The Geological Society of America. Available from: https://doi.org/10.1130/0-8137-2409-0.97

Kotthoff, U., Pross, J., Müller, U.C., Peyron, O., Schmiedl, G., Schulz, H. et al. (2008) Climate dynamics in the borderlands of the Aegean Sea during formation of sapropel S1 deduced from a marine pollen record. *Quaternary Science Reviews*, 27(7–8), 832–845.

Lacey, J.H., Francke, A., Leng, M.J., Vane, C.H. & Wagner, B. (2015) A high-resolution Late Glacial to Holocene record of environmental change in the Mediterranean from Lake Ohrid (Macedonia/Albania). *International Journal of Earth Sciences*, 104(6), 1623–1638.

Leng, M.J., Jones, M.D., Frogley, M.R., Eastwood, W.J., Kendrick, C.P. & Roberts, C.N. (2010) Detrital carbonate influences on bulk oxygen and carbon isotope composition of lacustrine sediments from the Mediterranean. *Global and Planetary Change,* 71, 175–182. https://doi.org/10.1016/j.gloplacha.2009.05.005

Lespez, L. (2003) Geomorphic responses to long-term land use changes in Eastern Macedonia (Greece). *Catena*, 51(3–4), 181–208.

Lolis, C.J., Bartzokas, A. & Katsoulis, B.D. (2002) Spatial and temporal 850 hPa air temperature and sea-surface temperature covariances in the Mediterranean region and their connection to atmospheric circulation. *International Journal of Climatology*, 22(6), 663–676.

Manning, S.W. (2013) The Roman world and climate: context, relevance of climate change, and some issues. In: Harris, W.V. (Ed.) *The ancient Mediterranean environment between science and history*. Leiden, The Netherlands: Brill, pp. 103–170.

Marcott, S.A., Shakun, J.D., Clark, P.U. & Mix, A.C. (2013) A reconstruction of regional and global temperature for the past 11,300 years. *Science*, 339(6124), 1198–1201.

Mastronuzzi, G., Calcagnile, L., Pignatelli, C., Quarta, G., Stamatopoulos, L. & Venisti, N. (2014) Late Holocene tsunamogenic coseismic uplift in Kerkira Island, Greece. *Quaternary International*, 332, 48–60.

Mayewski, P.A., Rohling, E.E., Curt Stager, J., Karlén, W., Maasch, K.A., Meeker, L.D. et al. (2004) Holocene climate variability. *Quaternary Research*, 62(3), 243–255.

Meyers, P.A. & Ishiwatari, R. (1993) Lacustrine organic geochemistry—an overview of indicators of organic matter sources and diagenesis in lake sediments. *Organic Geochemistry*, 20, 867–900.

Morellón, M., Anselmetti, F.S., Ariztegui, D., Brushulli, B., Sinopoli, G., Wagner, B. et al. (2016) Human–climate interactions in the central Mediterranean region during the last millennia: the laminated record of Lake Butrint (Albania). *Quaternary Science Reviews*, 136, 134–152.

Obrocki, L., Vött, A., Wilken, D., Fischer, P., Willershäuser, T., Koster, B. et al. (2020) Tracing tsunami signatures of the ad 551 and ad 1303 tsunamis at the Gulf of Kyparissia (Peloponnese, Greece) using direct push in situ sensing techniques combined with geophysical studies. *Sedimentology*, 67(3), 1274–1308. Available from: https://doi.org/10.1111/sed.12555

Philippson, A. (1959) *Die Griechischen Landschaften. Eine Landeskunde. Band III: Der Peloponnes*. Frankfurt: Klostermann, 523 pp.

Rasmussen, S.O., Andersen, K.K., Svensson, A.M., Steffensen, J.P., Vinther, B.M. & Clausen, H.B. et al. (2006) A new Greenland ice core chronology for the last glacial termination. *Journal of Geophysical Research: Atmospheres*, 111(D6), 1–16.

Reimer, P.J., Austin, W.E.N., Bard, E., Bayliss, A., Blackwell, P.G., Bronk Ramsey, C. et al. (2020) The IntCal20 Northern Hemisphere radiocarbon age calibration curve (0–55 cal kBP). *Radiocarbon*, 62(4), 725–757.

Rohling, E.J. & Pälike, H. (2005) Centennial-scale climate cooling with a sudden cold event around 8,200 years ago. *Nature*, 434(7036), 975–979.

Rohling, E.J., Hayes, A., Mayewski, P.A. & Kucera, M. (2009) Holocene climate variability in the Eastern Mediterranean, and the end of the Bronze Age. In: Bachhuber, C. & Roberts, G. (Eds.) *Forces of transformation: the end of the Bronze Age in the Mediterranean*. Oxford, UK: Oxbow Books, pp. 2–5.

Rohling, E.J., Marino, G. & Grant, K.M. (2015) Mediterranean climate and oceanography, and the periodic development of anoxic events (sapropels). *Earth-Science Reviews*, 143, 62–97.

Rohling, E.J., Marino, G., Grant, K.M., Mayewski, P.A. & Weninger, B. (2019) A model for archaeologically relevant Holocene climate impacts in the Aegean–Levantine region (easternmost Mediterranean). *Quaternary Science Reviews*, 208, 38–53.

Rothwell, R.G. (1989) The Smear Slide Method. In: Rothwell, R.G. (Ed.) *Minerals and mineraloids in marine sediments*. Dordrecht: Springer Netherlands, pp. 21–24.

Sapirstein, P. (2012) The monumental archaic roof of the temple of Hera at mon repos, Corfu. *The Journal of the American School of Classical Studies at Athens*, 81(1), 31–91.

Seguin, J., Bintliff, J.L., Grootes, P.M., Bauersachs, T., Dörfler, W., Heymann, C. et al. (2019) 2500 years of anthropogenic and climatic landscape transformation in the Stymphalia polje, Greece. *Quaternary Science Reviews*, 213, 133–154.

Siani, G., Magny, M., Paterne, M., Debret, M. & Fontugne, M. (2013) Paleohydrology reconstruction and Holocene climate variability in the South Adriatic Sea. *Climate of the Past*, 9(1), 499–515.

Sordinas, A. (1969) Investigations of the prehistory of Corfu during 1964–1966. *Balkan Studies*, 10, 393–424.

Thomas, E.R., Wolff, E.W., Mulvaney, R., Steffensen, J.P., Johnsen, S.J., Arrowsmith, C. et al. (2007) The 8.2ka event from Greenland ice cores. *Quaternary Science Reviews*, 26(1–2), 70–81.

Thucydides after Dent, J. M. (1910) *The Peloponnesian War*. New York: E.P. Dutton.

van Hinsbergen, D.J.J., van der Meer, D.G., Zachariasse, W.J. & Meulenkamp, J.E. (2006) Deformation of western Greece during Neogene clockwise rotation and collision with Apulia. *International Journal of Earth Sciences*, 95(3), 463–490.

Vött, A. (2007) Relative sea level changes and regional tectonic evolution of seven coastal areas in NW Greece since the mid-Holocene. *Quaternary Science Reviews*, 26(7–8), 894–919.

Vött, A. (2013) *Neue geoarchäologische Untersuchungen zur Verschüttung Olympias. Eine Einführung in die Olympia-Tsunami-Hypothese (OTH)*. 23. Trierer Winckelmannsprogramm 2011. Wiesbaden: Harrassowitz-Verlag, 51. p.

Vött, A., Brückner, H., May, S.M., Sakellariou, D., Nelle, O., Lang, F. et al. (2009) The Lake Voulkaria (Akarnania, NW Greece) palaeoenvironmental archive—a sediment trap for multiple tsunami impact since the mid-Holocene. *Zeitschrift für Geomorphologie, Supplementary Issues*, 53(1), 1–37. Available from: https://doi.org/10.1127/0372-8854/2009/0053S1-0001

Vött, A., Schriever, A., Handl, M. & Brückner, H. (2007) Holocene palaeogeographies of the eastern Acheloos River delta and the Lagoon of Etoliko (NW Greece). *Journal of Coastal Research*, 23/4, 1042–1066.

Weltje, G.J., Bloemsma, M.R., Tjallingii, R., Heslop, D., Röhl, U. & Croudace, I.W. (2015) Prediction of geochemical composition from XRF core dcanner data: a new multivariate approach including automatic selection of calibration samples and quantification of uncertainties. In: Croudace, I.W. & Rothwell, R.G. (Eds.) *Micro-XRF studies of sediment cores. Developments in Paleoenvironmental Research*, 17. Dordrecht: Springer Netherlands, pp. 507–534.

Weninger, B., Clare, L., Rohling, E., Bar-Yosef, O., Böhner, U., Budja, M. et al. (2009) The impact of rapid climate change on prehistoric societies during the Holocene in the Eastern Mediterranean. *Documenta praehistorica*, 36, 7–59.

Zanchetta, G., Borghini, A., Fallick, A.E., Bonadonna, F.P. & Leone, G. (2007) Late Quaternary palaeohydrology of Lake Pergusa (Sicily, southern Italy) as inferred by stable isotopes of lacustrine carbonates. *Journal of Paleolimnology*, 38(2), 227–239.

